A VLP vaccine platform comprising the core protein of hepatitis B virus with N-terminal antigen capture.

Kaniz Fatema*, Joseph S. Snowden*, Alexander Watson, Lee Sherry, Neil A. Ranson, Nicola J. Stonehouse# and David J. Rowlands#

Astbury Centre for Structural Molecular Biology, School of Molecular and Cellular Biology, Faculty of Biological Sciences, University of Leeds, Leeds, LS2 9JT, United Kingdom

* These authors contributed equally to the study.

Address correspondence to David J. Rowlands, D.J.Rowlands@leeds.ac.uk and Nicola J. Stonehouse, N.J.Stonehouse@leeds.ac.uk

Keywords: vaccine, platform, virus-like particle, ClearColi, HBcAg, Junín virus

Word count

Abstract: 159; Body text: 3,450 (including reference numbers)

Abstract

Nanoparticle presentation systems offer the potential to develop new vaccines rapidly in response to emerging diseases, a public health need that has become increasingly evident in the wake of the COVID-19 pandemic. Previously, we reported a nanoparticle scaffold system termed VelcroVax, comprising VLPs assembled from a tandem form of hepatitis B virus (HBV) core protein (HBc). This includes a high affinity SUMO binding protein (Affimer) able to recognise a SUMO peptide tag, inserted into the major immunodominant region. Here we describe a modified form of VelcroVax, comprising monomeric HBc with the Affimer inserted at the N-terminus (termed N-VelcroVax). N-VelcroVax VLPs expressed in *E. coli* effectively bind SUMO-tagged Junín virus glycoprotein, gp1 as assessed by structural and serological analyses. Cryo-EM characterisation of N-VelcroVax complexed with a SUMO-gp1 showed continuous density attributable to the fused Affimer, in addition to evidence of target antigen capture. Collectively, these data suggest that N-VelcroVax has potential as a versatile next generation vaccine scaffold.

Introduction

Virus vaccines developed by conventional means, e.g. attenuation or chemical inactivation, have been highly effective in reducing disease burdens in both humans and domesticated animals. However, advances in molecular biology and immunology in recent decades have expanded the options available for development of novel vaccines against intractable diseases and against newly emerging pathogens. Newer approaches to vaccine development include recombinant expression of protein subunits, recombinant live viral vectors, DNA, mRNA and nanoparticle vaccine platforms [1-3]. The original nanoparticle vaccines were virus-like particles (VLPs) produced by recombinant expression of self-assembling viral structural proteins. The first VLP vaccine to be licenced for human use was the hepatitis B surface antigen vaccine (HBsAg), which has been used to immunise many millions of people since its introduction in the 1980s [4, 5]. More recently, VLP vaccines have been successfully developed to immunise against human papillomavirus. These VLP vaccines provide immunity against the viruses from which the VLPs originated [6]. However, the principle of using VLPs as presentation systems for antigens derived from heterologous pathogens has been exemplified by the licencing of Mosquirix, which comprises HBsAg modified to include antigenic components of the malaria parasite [7]. In addition to viral structural proteins, other self-assembling proteins have been shown to produce nanoparticles suitable for chemical modification to provide candidate vaccine platforms [8, 9].

VLPs lack viral genetic material and therefore have no replicative ability and are intrinsically safe. Additionally, due to their structural resemblance to native viruses, VLPs inherently possess “self-adjuvanting” immunogenic properties to elicit a strong immune response. Moreover, VLPs are able to elicit both humoral and cellular immune responses initiating the production of specific antibodies and activating cytotoxic T-cells [10-13]. In addition to acting as antigens themselves, VLPs can be modified to display foreign epitopes [14-16]. A key

advantage of using VLP-based vaccine platforms is the ability to present antigens in a dense, highly repetitive manner, which leads to cross-linking of B cell receptors (BCRs) and B cell activation. Many studies have shown that VLP-based vaccines containing multivalent antigens elicit robust B cell activation and signalling and induce more effective immune responses than monovalent antigens [11, 13, 17, 18].

The capsid (or core) protein of hepatitis B virus (HBc) readily forms icosahedral VLPs when expressed in a wide range of prokaryotic and eukaryotic systems, which are inherently highly immunogenic. Consequently, the HBc VLP system has long been investigated as a potential vaccine platform [14, 15, 19-21]. The HBc protein comprises 183-185 amino acids (depending on genotype) and dimerises to produce structural subunits which assemble to form icosahedral VLPs with T = 3 (90 dimers) or T = 4 (120 dimers) morphologies [22]. The dimeric assembly results in the formation of 4 helix bundles (spikes) which project from the particle surface and a sequence at the tips of the spikes comprises the major immunodominant region (MIR). The MIR has been used as a preferred site for insertion of foreign epitopes because of its immunodominance [16, 23, 24] but this also poses challenges. There is a potential for steric clashes when two closely located copies of the inserted sequence are present at the tips of the spikes [23, 25]. Furthermore, insertion of large or hydrophobic sequences can interfere with the assembly of HBc particles and abrogate VLP formation [26, 27]. We previously addressed this problem by fusing two copies of HBc protein to produce tandem HBc VLPs, which allows the insertion of a foreign sequence into one MIR, leaving the other MIR in the tandem partner unmodified, resulting in the presence of only one foreign epitope per spike [23]. This approach allowed us to develop VelcroVax, incorporating an antigen capture sequence, an Affimer (a non-antibody high affinity artificial binding protein), inserted at a single MIR per spike [16]. Although these constructs form VLPs when expressed in eukaryotic systems, such as yeast or plants, they do not assemble efficiently when expressed in *E.coli*. Consequently, here we have

developed an alternative universal antigen capture platform for production in *E.coli*. In order to reduce the inherent anti-hepatitis B virus immunogenicity of the VLPs we modified the natural HBc protein sequence by inserting 5 additional amino acids within the MIR and refer here to this construct as wild type (wt) HBc 190. This construct was in turn modified to include an Affimer fused to the N-terminus instead of the MIR and termed N-VelcroVax. As an exemplar, we have demonstrated that the resulting VLPs efficiently bound a viral glycoprotein (Junín gp1) bearing the appropriate affinity tag.

Results

Expression of N-VelcroVax in *E. coli*

We previously generated a tandem HBc system, in which two copies of HBc protein are genetically linked and an anti-SUMO Affimer is inserted into the MIR of one of the HBc monomers (termed VelcroVax). This was able to bind SUMO-tagged target antigens for presentation as a multimeric VLP vaccine candidate [16]. Here, we have modified a monomeric HBc protein containing a 5 amino acid insertion into the MIR, termed wt HBc 190 (Fig.1A), by introducing the anti-SUMO Affimer sequence (Fig. 1C) at the N-terminus to produce N-VelcroVax (Fig 1B). This protein was expressed in *E.coli*, using the ClearColi BL21 (DE3) strain to minimise contamination with bacteria-derived pyrogens. Both wt HBc 190 and N-VelcroVax were efficiently expressed, as demonstrated by Western Blot analysis using anti-HBc (10E11) antibodies (Fig. 1D), with proteins of 22 kDa and 35 kDa detected, as expected. A minor band apparent in the N-VelcroVax lane is likely to be a degradation product.

N-VelcroVax assembles into icosahedral VLPs.

After confirmation of expression of N-VelcroVax in ClearColi BL21 (DE3) *E. coli* cells, cell extracts were purified by differential ultra-centrifugation including separation of assembled VLPs on sucrose gradients. Gradient fractions were then analysed by Western blot which confirmed the presence of N-VelcroVax in the middle fractions of the gradient, the expected position for Hbc VLPs (Fig. 2A) [16]. Examination of the peak fraction (fraction 5) by negative stain transmission electron microscopy (TEM) showed VLPs of the expected morphology (Fig. 2B).

Complexes of SUMO-gp1 and N-VelcroVax VLP co-sediment during sucrose gradient centrifugation.

We examined the SUMO-binding properties of N-VelcroVax VLP using a SUMO-tagged version of the gp1 protein of Junín virus (SUMO-gp1), which we had previously shown to bind to the tandem HBc version of VelcroVax [16]. For the initial investigation of binding, N-VelcroVax particles were mixed with SUMO-gp1 at a 1:1 molar ratio overnight at 4°C and separated by 15 - 45% sucrose gradient ultracentrifugation. The resulting fractions were analysed by Western blot using anti-HBc (10E11) or anti-Junín antibodies to detect the positions of N-VelcroVax (Fig 3, left) and SUMO-gp1 (Fig 3, right) in the gradients. Both HBc N-VelcroVax (35 kDa) and SUMO-gp1 (54 kDa) were present in the same gradient fractions, indicative of a strong non-covalent interaction (Fig 3). Excess unbound SUMO-gp1 was detected in the top gradient fractions (Fig 3, right).

Evaluation of SUMO-gp1 binding to N-VelcroVax by ELISA.

The SUMO-gp1 binding capacity of HBc N-VelcroVax was assessed by ELISA. SUMO-gp1 and HBc N-VelcroVax were mixed at molar ratios ranging from 1:1 to 5:1 before loading onto ELISA plates. After washing, the wells were interrogated with anti- HBc or anti-SUMO-gp1 antisera. The results indicated that N-VelcroVax particles strongly bound SUMO-gp1 with maximum binding occurring when the components were mixed at a 1:1 ratio (Fig. 4). No binding of SUMO-gp1 to wt HBc 190 VLPs was detected, as expected (Fig. 4)

Structural characterisation of N-VelcroVax and N-VelcroVax:SUMO-gp1 particles.

N-VelcroVax samples were vitrified for cryo-EM data collection (Fig S1, Table S1). This confirmed two different sizes of icosahedral particles, and reconstructions of each particle stack with icosahedral symmetry imposed revealed that these corresponded to T = 3 and T = 4 configurations, as expected.

Interestingly, both reconstructions (resolved to ~3.5 Å and ~3.3 Å, respectively) showed continuous densities allocated between four-helix bundles on the surface of the VLPs (Fig.5).

Each of these densities was of appropriate dimension to accommodate an Affimer and were located close to the residue at the N-terminus of a wt HBc 190 monomer, as expected. Unstructured internal density was also observed, possibly representing non-specific binding of nucleic acid derived from the *E.coli* expression system (Fig.5).

Next, we attempted to visualise N-VelcroVax VLPs in complex with a SUMO-tagged antigen, specifically, the gp1 glycoprotein of Junín virus (SUMO-gp1). Initial screening by negative stain TEM of N-VelcroVax:SUMO-gp1 complexes formed in solution revealed significant aggregation, so an alternative on-grid binding approach was pursued (i.e. separate samples of N-VelcroVax and SUMO-gp1 were applied directly to the grid in sequence). This showed no evidence of aggregation of N-VelcroVax particles and visual inspection suggested that the boundaries of the VLPs had become less well defined, indicative of some level of binding (Fig 6A).

This on-grid binding approach was subsequently used to prepare samples for cryo-EM analysis of N-VelcroVax:SUMO-gp1 samples (Fig S2, Table S1). Processing of cryo-EM data yielded density maps for T = 3 and T = 4 VLPs resolved to 3.0 Å and 3.5 Å, respectively. Initial inspection of density maps revealed no additional density attributable to bound SUMO-gp1, although there appeared to be a subtle change in the orientations of the Affimers, with these being closer together in the N-VelcroVax:SUMO-gp1 complex map compared to the unliganded N-VelcroVax map (Fig 6B).

Hypothesising that SUMO-gp1 was bound at a low occupancy, we attempted to resolve density for SUMO-gp1 by performing focussed classification, as described previously [28-31]. A mask was applied to a single Affimer and the volume expected to contain SUMO-gp1 for both T = 3 and T = 4 VLPs (Fig S3). Interestingly, several focussed classes revealed low-resolution density continuous with Affimer density, suggesting that SUMO-gp1 had been captured by N-

VelcroVax Affimers but was only present at a low occupancy (Fig 6C). Interestingly, density corresponding to the SUMO-gp1-binding Affimer in asymmetric reconstructions of focussed classes had reoriented upwards, suggesting that movement of the Affimer was necessary to accommodate the size of SUMO-gp1 (Fig 6D).

Discussion

The development of vaccine platforms suitable for multimeric presentation of antigenic components of important pathogens, so maximising their immune recognition, is an attractive approach toward novel vaccines. To this end, we produced recombinant HBc VLPs (N-VelcroVax) with an anti-SUMO Affimer genetically fused at the N-terminus of HBc190 protein. Although HBc VLPs have been expressed in a number of expression systems, e.g., insect cells, mammalian cells, plants, yeast [6, 11, 13, 24, 32], using low cost expression systems would make the VLPs accessible more widely, especially for lower-to-middle income countries (LMICs). Hence, we opted for a cost-effective *E. coli* expression system which offers simple, fast and inexpensive production, ease of in-process control and high productivity [6, 13, 32-35]. However, contamination with high levels of endotoxin derived from the *E. coli* cell wall is a major drawback of this expression system [34, 36-38]. To address this problem, we used ClearColi BL21 (DE3) *E. coli* cells for expression of N-VelcroVax. A previous study showed that using ClearColi BL21 (DE3) *E. coli* for expression of apolipoprotein A and heat shock protein 70 significantly reduced endotoxin level as measured by LAL assay (10 μg/mL) and did not trigger endotoxic responses in HEK-Blue hTLR4 cells [36]. The endotoxin content of N-VelcroVax expressed in ClearColi BL21 (DE3) *E. coli* was 10.2 EU/mL as assessed by LAL assay, which is half the maximum recommended level of endotoxin acceptable for subunit vaccines [34, 36, 39]. The N-VelcroVax VLPs bound SUMO Junín gp1 effectively with maximal binding occurring when the components were mixed at a 1:1 molar ratio (Fig. 4).

Examination by negative stain transmission electron microscopy showed that the morphology of the N-VelcroVax VLPs was as expected [40, 41]. Cryo-EM analysis of the VLPs revealed particles in both $T = 3$ and $T = 4$ configurations, as expected. In our earlier analyses of tandem core VelcroVax VLPs Affimer density was not visible, likely as a result of the location of the Affimers on flexible linkers at the tips of four-helix bundles [16]. However, for N-VelcroVax,

in which Affimers are attached at the N-terminus and spatially constrained between the four-helix bundles, Affimer density was resolved. This suggests that the Affimers in the N-VelcroVax system are more rigidly constrained in their position compared to when present at the MIR region.

N-VelcroVax was also visualised in complex with SUMO-gp1. Although SUMO-gp1 density was not resolved in symmetric reconstructions, focussed classification revealed low-resolution density continuous with Affimer density. This finding is suggestive of low occupancy, with the majority of unoccupied sites leading to the 'averaging out' of SUMO-gp1 density in symmetric reconstructions, possibly as a result of the on-grid binding method used during grid preparation. Interestingly, an asymmetric reconstruction derived from particles belonging to a single focussed class revealed that the corresponding Affimer had undergone a major reorientation in order to accommodate the target antigen, indicative of steric hindrance.

Conclusion

A flexible antigen presentation system, N-VelcroVax, was produced by genetic fusion of a SUMO-Affimer capture moiety at the N-terminus of HBc protein. Purified N-VelcroVax VLPs expressed in ClearColi BL21 (DE3) *E. coli* contained less endotoxin than the recommended maximum level for subunit vaccines due to modification of lipid A component of ClearColi cell membrane which is responsible for the endotoxic response. VLP-based vaccines, including HBc-VLPs have potential for the development of next generation vaccines and future immunisation experiments will determine the efficacy of N-VelcroVax VLPs as platforms to display immunogens.

Materials and methods

Expression constructs

An anti-SUMO-Affimer sequence was genetically fused at the N-terminus of wt HBc 190 to produce N-VelcroVax (Fig. 2). This was subcloned into the pET29b expression vector using *Nde*I and *Xho*I and transformed into *E. coli* DH5α chemically competent cells for plasmid propagation.

For the target protein, Junín gp1, a SUMO-His6 tag [16] was genetically fused to the N-terminus of the Junín virus glycoprotein 1 to form SUMO-Junín gp1 (kindly supplied by Thomas A. Bowden, University of Oxford, UK). This protein was expressed in mammalian cells.

Expression and purification of N-VelcroVax

ClearColi BL21 (DE3) *E. coli* was transformed with the N-VelcroVax plasmid and used for protein expression. N-VelcroVax plasmid was mixed with ClearColi BL21 (DE3) *E. coli* cells and incubated on ice for 30 min before being transferred to a 42 °C heat block for 50 seconds. Heat-shock transformed cells were then plated on LB-Agar plates (30 µg/mL kanamycin) and incubated overnight at 37 °C. A single colony was picked and cultured in 10 mL starter LB culture (30 µg/mL kanamycin) overnight at 37 °C and shaking at 200 rpm. The preculture was diluted 1:1000 into 500 mL LB (30 µg/mL kanamycin) and cultured at 37 °C, 200 rpm until OD_{600} ~0.6 – 0.8. Protein expression was induced with isopropyl β-D-1-thiogalactopyranoside (IPTG) (0.1 µM) and incubated at 18 °C, 200 rpm for a further 7 hours. The culture was centrifuged at 4000 x *g* for 10 minutes and the pellet was lysed with chemical lysis buffer. N-VelcroVax VLPs were purified by sedimentation through a 30% sucrose cushion followed by 15-45% sucrose gradient ultracentrifugation. The fractions containing the purified particles were analysed by SDS-PAGE. The concentration of purified N-VelcroVax was measured using

bicinchoninic acid (BCA) assay (Pierce) which revealed a yield of protein ~6.5 mg/L and endotoxin content of 10.2 EU/mL (Pierce LAL Chromogenic Endotoxin Quantitation kit; Thermo Scientific). Purified N-VelcroVax VLPs were stored at 4°C.

Negative-stain electron microscopy

Samples were prepared for negative-stain transmission EM by application to carbon-coated 300-mesh copper grids (Agar Scientific, UK) that had been glow discharged in air at 10 mA for 30 seconds immediately before use. Where N-VelcroVax or SUMO-gp1 was imaged alone, 3 µl of sample was applied directly to the grid surface for 30 seconds before washing and staining. To probe the interaction of N-VelcroVax with SUMO-gp1, the ligand was applied directly to the grid surface for 30 seconds after first applying N-VelcroVax and blotting away excess fluid. Following sample application, excess fluid was wicked away before grids were washed twice with 10 µl dH_2O. To stain the sample, 10 µl 1-2% uranyl acetate solution was applied to the grid and immediately removed by blotting, before an additional 10 µl 1-2% uranyl acetate solution was applied for 30 seconds. Grids were blotted to leave a thin film of stain and left to air dry.

Imaging was performed using an FEI Tecnai F20 transmission EM (operating at 200 kV with a field emission gun), equipped with an FEI CETA camera (Astbury Biostructure Laboratory, University of Leeds). Data were collected at various defocus values (-2.0 µm to -5.0 µm) at a nominal magnification of 25,000× giving an object sampling of 0.418 nm/pixel.

Cryo-electron microscopy

N-VelcroVax (in the presence or absence of target antigen) was vitrified using a LEICA EM GP plunge freezing device (Leica Microsystems, Wetzlar, Germany) in preparation for imaging by cryo-EM. Lacey carbon 400-mesh copper grids coated with a <3-nm continuous carbon film (Agar Scientific, UK) were glow discharged in air at 10 mA for 30 seconds prior to the

application of 3 µl N-VelcroVax (or N-VelcroVax:SUMO-gp1). For N-VelcroVax:SUMO-gp1, an on-grid interaction approach was used, such that following the application of VLP, excess fluid was manually blotted away and 3 µl SUMO-gp1 was applied. The sample was incubated on the grid surface for 30 seconds at 80% relative humidity (8°C) before excess fluid was blotted for a duration between 1 – 4 seconds and the grid vitrified in liquid ethane (cooled to –179°C by liquid nitrogen). Grids were transferred to liquid nitrogen for storage prior to clipping and imaging with an FEI Titan Krios TEM (Astbury Biostructure Laboratory, University of Leeds). Data collection was performed in integrating mode at a magnification of 75,000× (calibrated object sampling of 1.065 Å/pixel) with the microscope operating at 300 kV (a full set of data collection parameters is provided in Table S1).

Image Processing

Image processing was performed in Relion-3.0 and Relion-3.1 [42-44]. Following motion correction and CTF estimation of micrographs [44, 45], a subset of manually picked particles was subjected to 2D classification, and class averages were used as templates for automated particle picking. Initial particle stacks generated by automated picking were down-sampled (2x for N-VelcroVax, 4x or 5x for N-VelcroVax:SUMO-gp1) before several rounds of 2D classification to progressively remove junk particles and separate T = 3 and T = 4 VLPs. To reduce computational load, the first 2D classification was performed with CTFs ignored until the first peak, and maximum signal limited to 200. T = 3 and T = 4 particles were separately re-extracted without down-sampling for independent 3D refinement of each VLP configuration (with I1 symmetry imposed), based on initial models generated *de novo* in Relion. For each reconstruction, map quality was improved with iterations of CTF refinement and Bayesian polishing. Final refinements were performed with a solvent-excluding mask and flattened Fourier shell correlation (FSC) calculations. This was followed by mask-based sharpening, determination

of nominal resolution using the gold-standard FSC criterion (FSC = 0.143), and calculation of local resolution for each map.

Focussed classification was performed using 2x down-sampled data to limit the computational load, following a previously described protocol [28]. Briefly, a cylindrical mask was generated in SPIDER [46] and placed manually over a single Affimer and the space distal to it, expected to contain density for SUMO-gp1, using UCSF Chimera [47]. Relion was used to apply a soft edge to the mask, and to generate symmetry-expanded stacks of particles based on the orientational information generated during separate symmetrised 3D refinements for T = 3 and T = 4 VLPs. Symmetry expanded particle stacks were subjected to 3D classification without alignments, with the focussed mask applied. Asymmetric reconstructions were performed using Relion following focussed classification.

Enzyme-linked immunosorbent assay (ELISA)

A non-competitive indirect ELISA was developed to measure the binding capacity of N-VelcroVax vaccine scaffold to capture SUMO-tagged proteins using 96-well ELISA plates (Greiner Technologies, Bio-One, UK). The plate was coated with N-VelcroVax at 2.5 ug/mL (125 ng/well) and incubated overnight at 4 °C. The plate was blocked with blocking buffer (PBS + 2% skim milk) for 1 h at room temperature (RT) and then incubated with the SUMO-tagged protein (e.g., Junín gp1, SARS-CoV-2) for 1 hour at RT. Specific primary antibodies (mouse monoclonal anti-HBc (Abcam ab8639), anti-Junín gp1 (NR 2567),) were added and incubated for 1 hour at RT. The bound primary antibodies were detected with HRP-conjugated goat anti-mouse IgG and incubated for 1 hour at RT. Subsequently, chromogenic substrate TMB (ThermoFisher, Waltham, MA, USA) was added and incubated for 20 minutes at RT. The plates were washed with wash buffer (PBS + 1% Tween 20) four times between each step.

The reaction was stopped by 2 M H_2SO_4 (50 µl/well) and plates then analysed using a Biotech PowerWave XS2 plate reader.

Acknowledgments

We thank other members of the Stonehouse/Rowlands group at the University of Leeds for their insightful contributions. We also thank Professor Tom Bowden and Dr Guido Paesen, University of Oxford who provided SUMO-gp1.

Funding

This work was supported by a Wellcome PhD studentship to J.S.S. (102174/B/13/Z). Electron microscopy was performed in the Astbury Biostructure Laboratory, which was funded by the University of Leeds and Wellcome (108466/Z/15/Z).

Conflict of Interest

The authors declare that there is no conflict of interest.

Authors and Contributions

K.F., J.S.S., N.J.S., and D.J.R. conceived and designed the experiments. K.F. and L.S. generated the N-VelcroVax sequence. K.F. introduced this into ClearColi BL21 (DE3) cells, generated material for the characterisation of N-VelcroVax and performed serological characterisation. J.S.S. performed negative stain EM and cryo-EM. J.S.S. and A.W. processed and analysed cryo-EM data. N.A.R., D.J.R. and N.J.S. provided supervision. K.F., J.S.S., L.S., D.J.R., & N.J.S. wrote and edited the manuscript. Funding was secured for this research by N.A.R. and N.J.S.

References

1. Amanna, I. and M. Slifka, *Vaccination Strategies against Highly Variable Pathogens.* Current Topics in Microbiology and Immunology. Springer International Publishing, 2018: p. 1-30.
2. Delany, I., R. Rappuoli, and E. De Gregorio, *Vaccines for the 21st century.* EMBO molecular medicine, 2014. **6**(6): p. 708-720.
3. Nandy, A. and S.C. Basak, *Bioinformatics in design of antiviral vaccines.* Encyclopedia of Biomedical Engineering, 2019: p. 280.
4. Krugman, S. and M. Davidson, *Hepatitis B vaccine: prospects for duration of immunity.* The Yale journal of biology and medicine, 1987. **60**(4): p. 333.
5. Brenzel, L., et al., *Vaccine-preventable diseases.* Disease control priorities in developing countries, 2006. **2**: p. 389-412.
6. Gu, Y., et al., *Characterization of an Escherichia coli-derived human papillomavirus type 16 and 18 bivalent vaccine.* Vaccine, 2017. **35**(35): p. 4637-4645.
7. Laurens, M.B., *RTS, S/AS01 vaccine (Mosquirix™): an overview.* Human vaccines & immunotherapeutics, 2020. **16**(3): p. 480-489.
8. Nguyen, B. and N.H. Tolia, *Protein-based antigen presentation platforms for nanoparticle vaccines.* npj Vaccines, 2021. **6**(1): p. 70.
9. Tariq, H., et al., *Virus-like particles: Revolutionary platforms for developing vaccines against emerging infectious diseases.* Frontiers in microbiology, 2022. **12**: p. 790121.
10. Crisci, E., J. Bárcena, and M. Montoya, *Virus-like particles: the new frontier of vaccines for animal viral infections.* Veterinary immunology and immunopathology, 2012. **148**(3-4): p. 211-225.
11. Nooraei, S., et al., *Virus-like particles: preparation, immunogenicity and their roles as nanovaccines and drug nanocarriers.* Journal of nanobiotechnology, 2021. **19**(1): p. 1-27.
12. Ulrich, R., et al., *Core particles of hepatitis B virus as carrier for foreign epitopes.* Advances in virus research, 1998. **50**: p. 141-182.
13. Huang, X., et al., *Escherichia coli-derived virus-like particles in vaccine development.* npj Vaccines, 2017. **2**(1): p. 1-9.
14. Gregson, A.L., et al., *Phase I trial of an alhydrogel adjuvanted hepatitis B core virus-like particle containing epitopes of Plasmodium falciparum circumsporozoite protein.* PloS one, 2008. **3**(2): p. e1556.
15. Kutscher, S., et al., *Design of therapeutic vaccines: hepatitis B as an example.* Microbial biotechnology, 2012. **5**(2): p. 270-282.
16. Kingston, N.J., et al., *VelcroVax: a "Bolt-On" Vaccine Platform for Glycoprotein Display.* Msphere, 2023. **8**(1): p. e00568-22.
17. Kushnir, N., S.J. Streatfield, and V. Yusibov, *Virus-like particles as a highly efficient vaccine platform: diversity of targets and production systems and advances in clinical development.* Vaccine, 2012. **31**(1): p. 58-83.
18. Pumpens, P. and E. Grens, *HBV core particles as a carrier for B cell/T cell epitopes.* Intervirology, 2001. **44**(2-3): p. 98-114.
19. Whitacre, D.C., B.O. Lee, and D.R. Milich, *Use of hepadnavirus core proteins as vaccine platforms.* Expert review of vaccines, 2009. **8**(11): p. 1565-1573.
20. Pang, E.L., et al., *Epitope presentation of dengue viral envelope glycoprotein domain III on Hepatitis B core protein virus-like particles produced in Nicotiana benthamiana.* Frontiers in plant science, 2019. **10**: p. 455.
21. Ravin, N., et al., *Plant-produced recombinant influenza vaccine based on virus-like HBc particles carrying an extracellular domain of M2 protein.* Biochemistry (Moscow), 2012. **77**(1): p. 33-40.
22. Petrovskis, I., et al., *Production of the HBc Protein from Different HBV Genotypes in E. coli. Use of Reassociated HBc VLPs for Packaging of ss-and dsRNA.* Microorganisms, 2021. **9**(2): p. 283.

374 23. Peyret, H., et al., *Tandem fusion of hepatitis B core antigen allows assembly of virus-like*
375 *particles in bacteria and plants with enhanced capacity to accommodate foreign proteins.*
376 PLoS One, 2015. **10**(4): p. e0120751.
377 24. Stephen, S.L., et al., *Recombinant expression of tandem-HBc virus-like particles (VLPs)*, in *Virus-*
378 *Derived Nanoparticles for Advanced Technologies*. 2018, Springer. p. 97-123.
379 25. Wang, W., et al., *Major immunodominant region of Hepatitis B virus core antigen as a delivery*
380 *vector to improve the immunogenicity of the fusion antigen ROP2-SAG1 multiepitope from*
381 *Toxoplasma gondii in Mice.* Viral immunology, 2017. **30**(7): p. 508-515.
382 26. Shepherd, D.A., et al., *Using ion mobility spectrometry–mass spectrometry to decipher the*
383 *conformational and assembly characteristics of the hepatitis B capsid protein.* Biophysical
384 journal, 2013. **105**(5): p. 1258-1267.
385 27. Karpenko, L., et al., *Insertion of foreign epitopes in HBcAg: how to make the chimeric particle*
386 *assemble.* Amino acids, 2000. **18**: p. 329-337.
387 28. Scheres, S.H., *Processing of structurally heterogeneous cryo-EM data in RELION.* Methods in
388 enzymology, 2016. **579**: p. 125-157.
389 29. Conley, M.J., et al., *Calicivirus VP2 forms a portal-like assembly following receptor*
390 *engagement.* Nature, 2019. **565**(7739): p. 377-381.
391 30. Snowden, J.S., et al., *Dynamics in the murine norovirus capsid revealed by high-resolution cryo-*
392 *EM.* PLoS Biology, 2020. **18**(3): p. e3000649.
393 31. Snowden, J.S., et al., *Structural insight into Pichia pastoris fatty acid synthase.* Scientific
394 Reports, 2021. **11**(1): p. 9773.
395 32. Naskalska, A. and K. Pyrć, *Virus like particles as immunogens and universal nanocarriers.* Polish
396 journal of microbiology, 2015. **64**(1).
397 33. Zhu, J., *Mammalian cell protein expression for biopharmaceutical production.* Biotechnology
398 advances, 2012. **30**(5): p. 1158-1170.
399 34. Schwarz, H., et al., *Residual endotoxin contaminations in recombinant proteins are sufficient*
400 *to activate human CD1c+ dendritic cells.* PLoS One, 2014. **9**(12): p. e113840.
401 35. Kniskem, P.J., et al., *Unusually high-level expression of a foreign gene (hepatitis B virus core*
402 *antigen) in Saccharomyces cerevisiae.* Gene, 1986. **46**(1): p. 135-141.
403 36. Mamat, U., et al., *Detoxifying Escherichia coli for endotoxin-free production of recombinant*
404 *proteins.* Microbial cell factories, 2015. **14**(1): p. 1-15.
405 37. Demain, A.L. and P. Vaishnav, *Production of recombinant proteins by microbes and higher*
406 *organisms.* Biotechnology advances, 2009. **27**(3): p. 297-306.
407 38. Khow, O. and S. Suntrarachun, *Strategies for production of active eukaryotic proteins in*
408 *bacterial expression system.* Asian Pacific journal of tropical biomedicine, 2012. **2**(2): p. 159-
409 162.
410 39. Brito, L.A. and M. Singh, *Commentary: acceptable levels of endotoxin in vaccine formulations*
411 *during preclinical research.* Journal of pharmaceutical sciences, 2011. **100**(1): p. 34-37.
412 40. Lua, L.H., et al., *Bioengineering virus-like particles as vaccines.* Biotechnology and
413 bioengineering, 2014. **111**(3): p. 425-440.
414 41. Heider, S. and C. Metzner, *Quantitative real-time single particle analysis of virions.* Virology,
415 2014. **462**: p. 199-206.
416 42. Scheres, S.H., *RELION: implementation of a Bayesian approach to cryo-EM structure*
417 *determination.* Journal of structural biology, 2012. **180**(3): p. 519-530.
418 43. Zivanov, J., et al., *New tools for automated high-resolution cryo-EM structure determination*
419 *in RELION-3. Elife 7. iCP (E)*. 2018, PA28αβ-iCP-PA28αβ.
420 44. Zheng, S.Q., et al., *MotionCor2: anisotropic correction of beam-induced motion for improved*
421 *cryo-electron microscopy.* Nature methods, 2017. **14**(4): p. 331-332.
422 45. Zhang, K., *Gctf: Real-time CTF determination and correction.* Journal of structural biology,
423 2016. **193**(1): p. 1-12.

46. Frank, J., et al., *SPIDER and WEB: processing and visualization of images in 3D electron microscopy and related fields.* Journal of structural biology, 1996. **116**(1): p. 190-199.
47. Pettersen, E.F., et al., *UCSF Chimera—a visualization system for exploratory research and analysis.* Journal of computational chemistry, 2004. **25**(13): p. 1605-1612.
48. Wynne, S., R. Crowther, and A. Leslie, *The crystal structure of the human hepatitis B virus capsid.* Molecular cell, 1999. **3**(6): p. 771-780.
49. Tiede, C., et al., *Affimer proteins are versatile and renewable affinity reagents.* Elife, 2017. **6**: p. e24903.

Figures

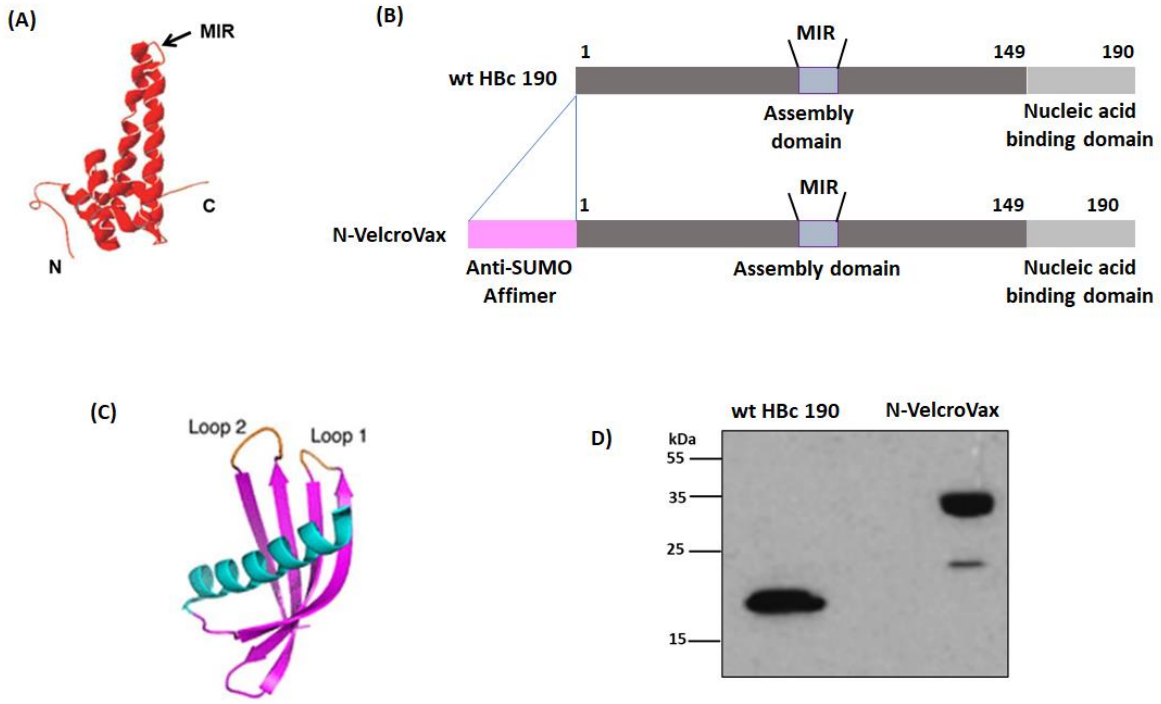

Figure 1: Characterisation of N-VelcroVax. (A) X-ray crystal structure of HBc monomer indicating the N-terminus, C-terminus and major immunodominant region (MIR) (PDB: 1QGT; ref. [48]). **(B)** wt HBc 190 construct (contains no anti-SUMO-Affimer) and N-VelcroVax, indicating the N- terminal insertion of the anti-SUMO-Affimer. **(C)** Crystal structure of an Affimer, non-antibody artificial binding protein, selected against human SUMO protein (PDB: 5ELJ). Loop 1 and Loop 2 are the variable regions [49]. **(D)** Small-scale expression of HBc VLPs: Western Blot of wt HBc 190 and N-VelcroVax expressed in ClearColi BL21 (DE3) *E. coli* cells detected with mouse monoclonal anti-HBc (10E11). The figure is a representative example of three separate experiments.

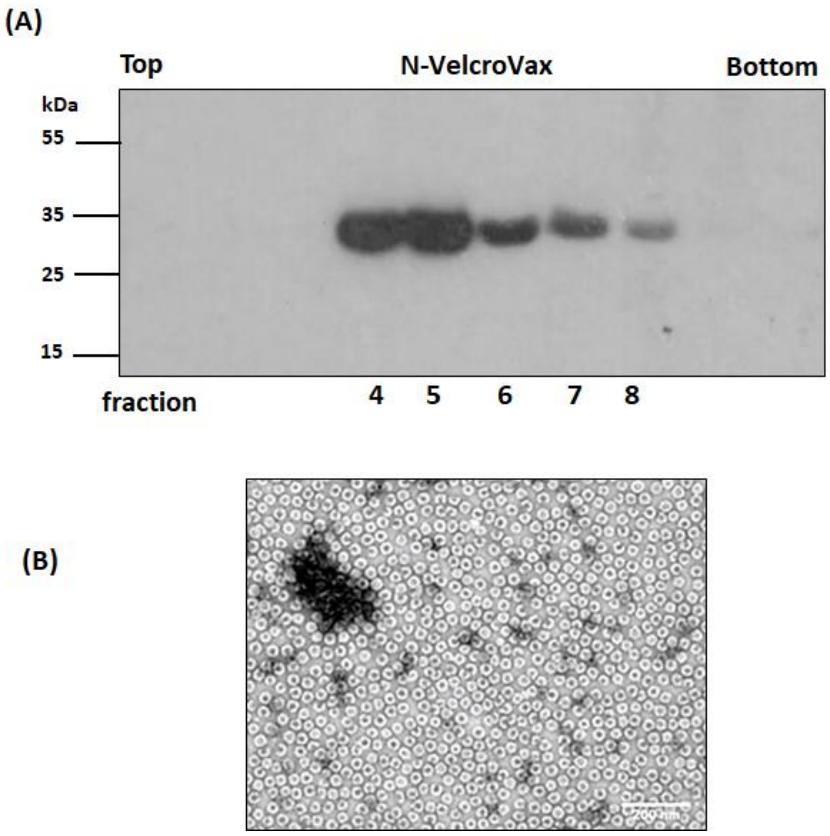

Figure 2. Purification and characterisation of N-VelcroVax particles. (A) Western blot of gradient purified N-VelcroVax particles, expressed in ClearColi BL21 (DE3) *E. coli* cells detected with mouse monoclonal anti-HBc (10E11). **(B)** TEM analysis of N-VelcroVax. The VLPs were stained using 2% uranyl acetate. The scale bar shows 200 nm. The figure is a representative example of three separate experiments.

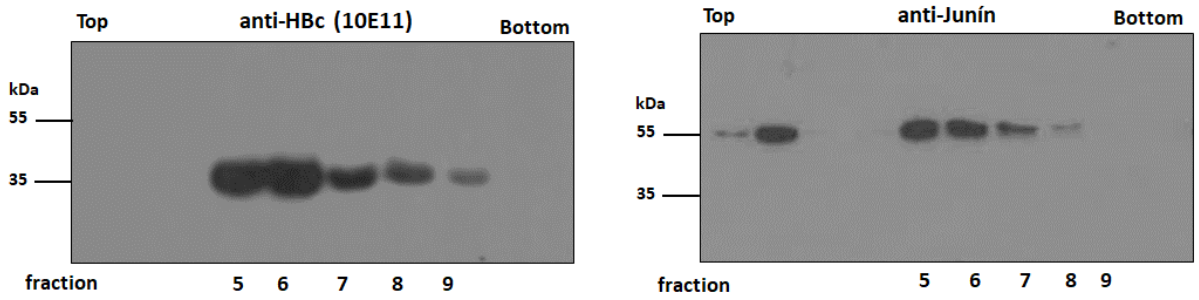

Figure 3. Evaluating the binding capacity of N-VelcroVax to SUMO-gp1. N-VelcroVax and SUMO-gp1 were mixed and incubated overnight before separation on a sucrose density gradient. Gradient fractions were analysed by Western blot using either mouse monoclonal anti-HBc (10E11, left) or anti-Junín (right). The figure is a representative example of three separate experiments.

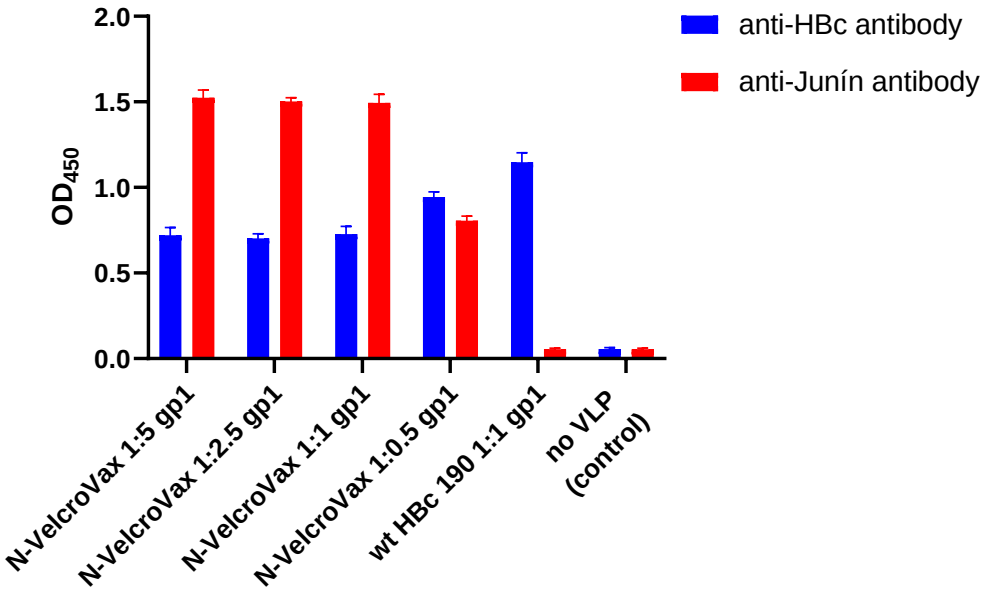

Figure 4. Evaluating the optimum molar ratio for interaction between N-VelcroVax and SUMO-gp1. N-VelcroVax and SUMO-gp1 were mixed in molecular ratios ranging from 1:1 to 1:5 and binding determined by ELISA. Anti-HBc 10E11 (1:1000) and anti-Junín (1:32,000) were used to detect HBc VLPs and SUMO-gp1 respectively. Anti-mouse antibody conjugated with HRP was added as secondary antibody. TMB chromogenic substrate was used to detect HRP. The optical density at 450 nm (OD 450 nm) is represented in arbitrary units (n = 3).

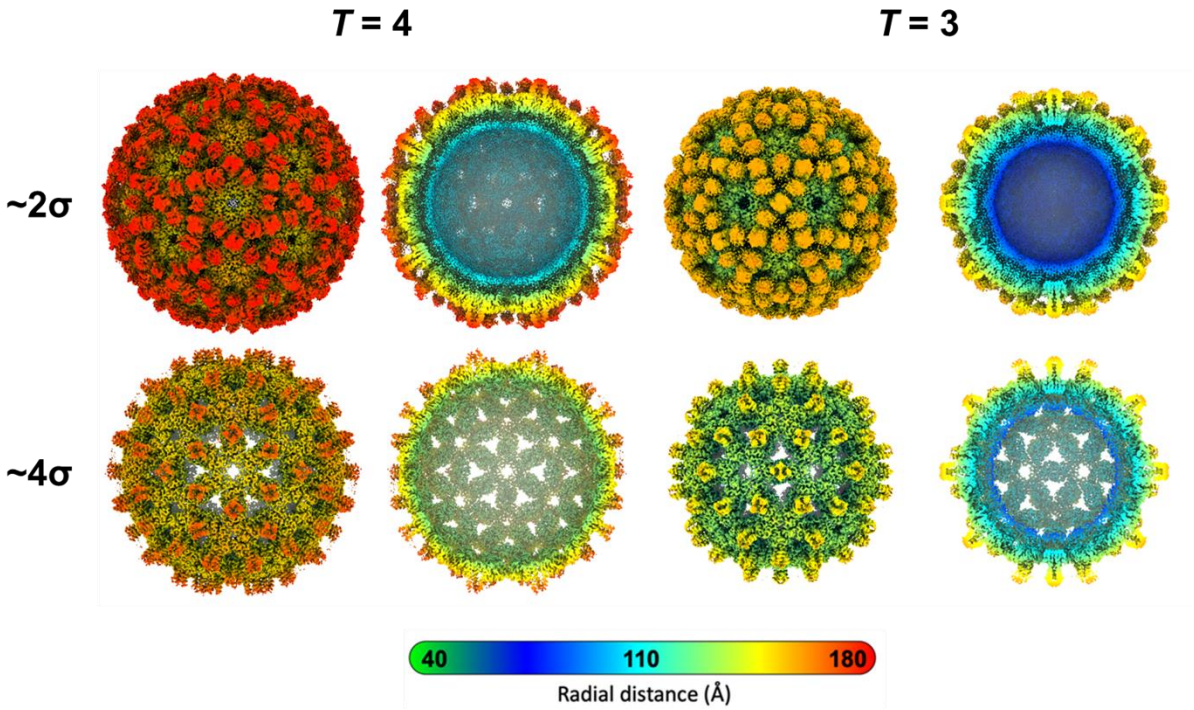

Figure 5. Characterisation of unconjugated N-VelcroVax VLPs by cryo-EM. Density maps for *T* = 4 (left) and *T* = 3 (right) N-VelcroVax reconstructions, filtered according to local resolution. Each density map is shown as a complete isosurface representation and central cross-section at both low (approx. 2σ, Affimer densities visible) and high (approx. 4σ, Affimer densities not visible) contour level. Cross-sectional views show density, potentially nucleic acid bound non-specifically to the interior surface of the VLPs. Maps are coloured by radial distance (Å).

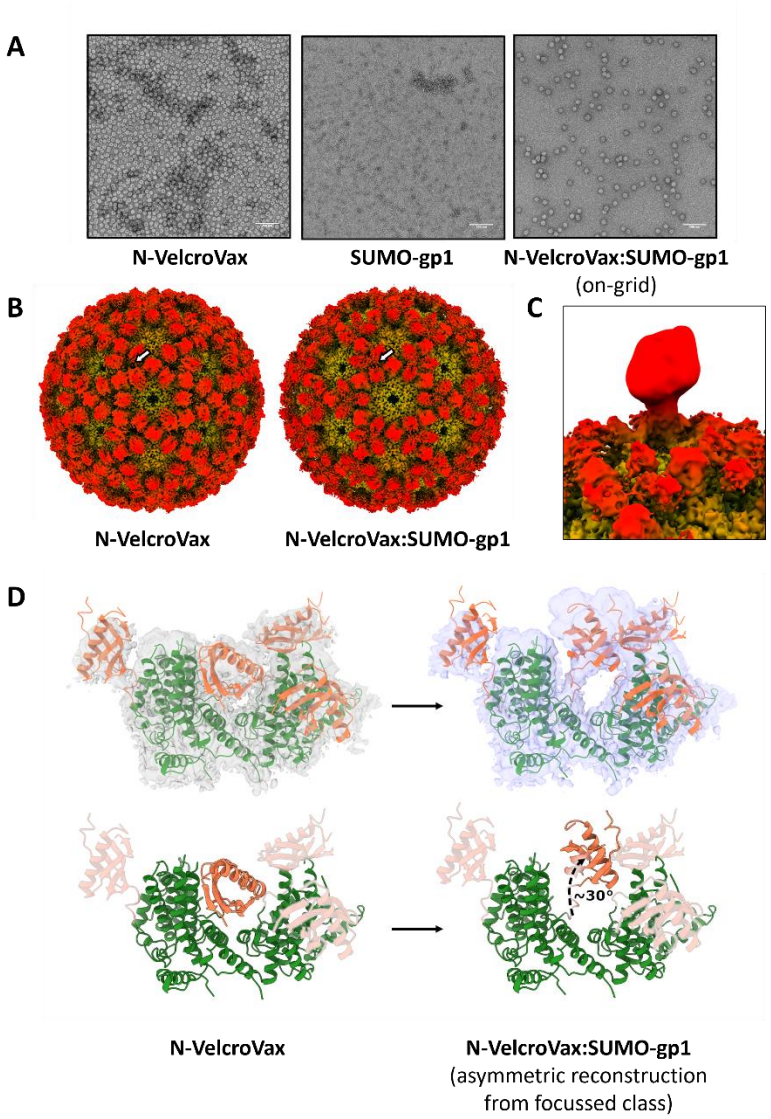

Figure 6. Structural characterisation of N-VelcroVax in complex with SUMO-gp1. (A) Representative micrographs from negative stain TEM analysis of N-VelcroVax alone (left), SUMO-gp1 alone (centre), or N-VelcroVax:SUMO-gp1 following on-grid interaction (right). Scale bars show 200 nm. **(B)** Isosurface representations of cryo-EM density maps for the T = 4 configuration of unliganded N-VelcroVax (left) and N-VelcroVax:SUMO-gp1 (right), shown at ~2 σ and coloured radially. Affimers show a subtle change in relative positioning, as indicated by the white arrow. **(C)** Asymmetric reconstruction of particles from a single focussed class following focussed classification of N-VelcroVax:SUMO-gp1 T = 4 particles, showing additional low-resolution density corresponding to bound SUMO-gp1. All focussed classes are shown in Fig S3. **(D)** Density from an asymmetric reconstruction of T = 4 N-VelcroVax:SUMO-gp1 following focussed classification (purple) is suggestive of a reorientation of the Affimer compared to its position in the unliganded N-VelcroVax density map (grey). Fitted atomic models (orange – Affimers, green – remainder of N-VelcroVax) are shown for illustrative purposes.